Laser Surface Textured PTFE Inhibitation for Stick-Slip Phenomenon Under Boundary Lubrication

*LEI Ming**, *WANG Xiaolei*, *HUANG Wei*

College of Mechanical and Electrical Engineering, Nanjing University of Aeronautics and Astronautics, Nanjing 210016, P.R.China

(Received 14 May 2021; revised 30 June 2021; accepted 5 July 2021)

Abstract: When the machine tool is in the start- and stop-stages, the stick-slip phenomenon will be observed and high-precision positioning, machining accuracy and fretting feed will not be guaranteed. The most critical reason is that there is the difference between the dynamic and the static friction coefficients. Textures with different area ratios are fabricated on the surfaces of the upper PTFE-based composite and the friction tests are carried out on a reciprocating tribotester under the boundary lubrication and flat-on-flat contact conditions. The results show that there exists an optimal textured area ratio of 19.6% that can minimize the difference between the dynamic and the static friction coefficients.

Key words: machine tool; laser surface texturing; stick-slip phenomenon; difference between the dynamic and static friction coefficients

CLC number: TH117 **Document code:** A **Article ID:** 1005-1120(2021)S-0093-09

0 Introduction

The machine tool is the most basic and important equipment in the manufacturing industry. However, with the rapid development of nano-processing technology, micro-machinery and micro-drive technology, higher requirements are placed on the machine tool: More complex component shapes, ultra-high positioning accuracy, inching feed positioning accuracy, stability of feed system and ultra-precision processing. The guide rail is one of the core components in the machine tool, which greatly determines the accuracy and precision[1]. The plastic-surface guide rail is a metal-to-plastic friction one. A sliding surface is covered with a layer of anti-wear soft tape, usually based on polytetrafluoroethylene (PTFE)[2]. They are widely used in various CNC machine tools. Compared with ordinary sliding guide rails, they have the advantages of low friction coefficient, long life, simple structure, low cost, good shock absorption and low noise[3]. However, at a low speed and a heavy load, the relative motion of the two contact surfaces is not continuous, but there are two states of adhension and sliding[4]. This kind of vibration-stabilized motion is called jerky motion or stick-slip phenomenon[5-7].

Especially when the machine tool is in the start- and stop-stages, under the boundary lubrication condition, due to the difference between the dynamic and the static friction coefficients in general, where the static friction force is larger than the dynamic friction force, the stick-slip phenomenon is more obvious. According to frictional mechanics, the reason why the stick-slip phenomenon occurs is the mechanical interaction between friction force and elasticity of the sliding pairs[8]. Friction is a shear force that resists the relative motion between two contacting surfaces, while elasticity is a property of a deformable mass to store mechanical energy. Consequently, elasticity of the sliding mass stores me-

*Corresponding author, E-mail address: mingleinuaa@hotmail.com.

How to cite this article: LEI Ming, WANG Xiaolei, HUANG Wei. Laser surface textured PTFE inhibitation for stick-slip phenomenon under boundary lubrication[J]. Transactions of Nanjing University of Aeronautics and Astronautics, 2021, 38(S): 93-101.

http://dx.doi.org/10.16356/j.1005-1120.2021.S.012

chanical energy during a stick phase, and this energy dissipates during the following slip phase[9]. The surface of the object is uneven, with bumps randomly distributed. When subjected to the shear force, these bumps will bond together to form micro-welded bridges. With the increase of the shear force, these micro-welded bridges will break and a relative sliding movement will occur. Therefore, the continuous formation and fracture of these micro-welded bridges lead to the stick-slip phenomenon. The main factors affecting the stick-slip phenomenon are the damping of the system, the transmission rigidity of the feed mechanism, the driving speed, the lubricating oil and the friction coefficient. If the stick-slip phenomenon is not avoided or inhibited, ultra-high-precision positioning cannot be achieved[10].

In recent decades, a great number of theoretical and practical studies have shown that by changing the morphology of the two contact surfaces, their tribological properties can be significantly improved. This concept can be traced back to 1966, proposed by Hamilton and Allen, who has conducted creative research on textured bearings and introduced the concept of "micro-irregularities"[11-12]. With the intensive study of texture, its application scope has gradually expanded, such as increasing the thickness of the lubricant film[13], reducing wear and improving engine life[14-15], increasing the load carrying capacity and reducing frictional resistance of bearings[16-18], and applying to new bionic surface texture designs[19]. Under lubricating conditions, the improvement of tribological performance through surface texture can be attributed to the following three reasons: Micro-hydrodynamic effect, secondary lubrication and wear debrises trapping action[20].

However, few people apply texture to the surface of the machine guide rail, especially by processing the texture on the surface of the guide rail to inhibit stick-slip phenomenon of the guide rail to achieve ultra-high precision positioning and manufacturing. Yue et al. fabricated the grooves on the surface of guide rail made of AISI 1045 and AISI 5104 with the method of LST to study its inhibitory effect on stick and slip phenomenon during which the standard deviation of friction force was used as evaluation index[1]. The results showed that the lowest friction coefficient was achieved for both-side-textured guide rail, while only-one-side texture was more effective in preventing stick-slip motion. Wang et al. fabricated four different textures on GCr15 bearing steel by LST and used the critical speed as evaluation index[21]. The results showed that the critical stick-slip speed of bulge-textured surface is 95.9% lower than that of the smooth surface. When the reciprocating test is to be carried out, many scholars used the pin-on-disk or ball-on-disk instead, where the contact area was relatively small and unable to guarantee consistency with actual working conditions. There is little knowledge about a flat-on-flat contact condition.

Herein, laser surface texturing (LST) is used to process the texture on the surface of the PTFE-based composite, which is sticked to one side of the machine guide rail and the difference between the dynamic and static friction coefficients is used as evaluation index. The friction test is carried out by imitating the actual working conditions of the guide rail on the reciprocating friction test machine, among which the speed range spans two orders of magnitude. The test results show that by processing the texture on the soft PTFE tape, the stick-slip phenomenon can be significantly inhibited and a lower friction coefficient can be achieved to improve tribological properties.

1 Experiment

The lower guide rail with size of 100 mm×60 mm×10 mm is made of HT-250. The chemical composition of the guide rail used is shown in Table 1. The upper sample with size of 5 mm×5 mm×

Table 1 Chemical composition of the lower guide rail %

Sample	Material	Chemical range and limit				
		C	Si	Mn	S	P
Lower guide rail	HT-250	3.16—3.30	1.79—1.93	0.89—1.04	0.094—0.125	0.120—0.170

1 mm is Turcite®-B Slydway®, the properties of which are shown in Table 2. Then both the upper and lower samples are polished by the abrasive paper with the types of W28, W10, W5 to achieve the Ra (0.05±0.01) μm and cleaned ultrasonically with acetone subsequently. The CO_2 laser system is used to perform the LST with laser wavelength of 10.6 μm and laser power of 30 W. And the processing parameters are as follows: power of 24 W, frequency of 20 kHz, line spacing of 0.05 mm, scanning speed of 500 mm/s, beam diameter of 0.1 mm, and repeat times of 1. The dimple array patterns with different area ratios are fabricated on the surface of the upper samples and Fig.1 shows configuration of the dimple arrays and the scanning electron micrograph of surface topography, respectively. The upper samples with different area ratios are named S1, S2, S3, S4, S5, S6, S7, and S8, respectively, shown in Table 3 and in which n represents the number of dimples. To remove the burrs and bulges caused by the thermal effect of the LST around the dimples, the textured upper samples are polished by abrasive paper again and ultrasonic cleaned subsequently.

Table 2 Properties of the upper sample

Sample	Name	Main composition	Tension/(kg•cm^{-2})	Hardness	Coefficient of expansion	Maximum pressure/(kg•cm^{-2})
Upper PTFE-Belt	Turcite®-B Slydway®	PFTE	140	HRC45	6×10^{-2}	110

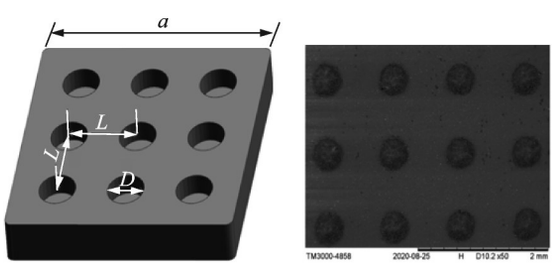

(a) Dimensional sketch of the textured sample

(b) Scanning electron micrograph of surface topography

Fig.1 Dimensional sketch of the textured sample and scanning electron micrograph of surface topography

Table 3 Parameters of different samples

No.	a/mm	D/mm	L/mm	n	Ratio/%
S1	5	0	0	0	0
S2	5	0.5	2.5	4	3.14
S3	5	0.5	1.5	9	7.03
S4	5	0.5	1.25	16	12.56
S5	5	0.5	1.0	25	19.6
S6	5	0.5	0.8	36	28.26
S7	5	0.5	0.7	49	38.46
S8	5	0.5	0.625	64	50.24

A reciprocating tribotester (Surface Measurement Machine, Sinto Scientific, Japan) shown in Fig.2 is used to perform the friction tests under boundary lubrication with the room temperature of 23 ℃ and relative humidity of 50%. The stroke length is set as 20 mm. The load is used by the standard weights. The upper sample is sticked to the

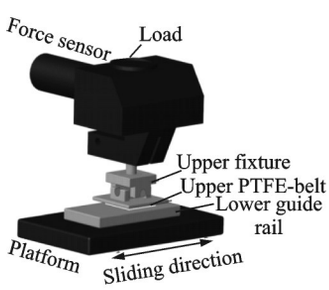

(a) Reciprocating tribotester

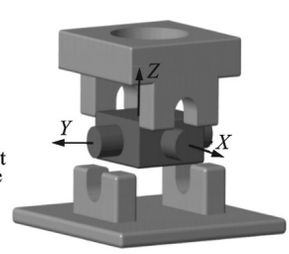

(b) Upper fixture

Fig.2 Reciprocating tribotester and upper fixture

specially designed upper fixture (Fig.2(b)) which can be adaptively adjusted to ensure that the upper and lower samples are in flat-on-flat contact during the friction tests. The core part of the upper fixture is the cross arm in the middle which prevents the movement in the X, Y, and Z directions and rotation around the Z axis. As a result, the upper sample can rotate 360° for adaptive adjustment but cannot rotate in X-Y plane which guarantees that the sliding direction cannot change during the friction tests. The lower sample is mounted on the reciprocating platform which is connected to a motion mechanism. MOBIL VACTRA OIL NO.2, a type of guide rail lubricating oil, is used as lubricant during the friction tests.

Before the friction tests, a 30 min pre-sliding is conducted with 0.2 ml of the oil lubricant to ensure that the dimple arrays are filled with the oil lubricant

and the running-in stage is finished. No additional oil lubricant is added during the tests to get the boundary lubrication condition. During the friction tests, the sliding speed is set to 0.1, 0.5, 1, 5, and 10 mm/s and the vertical load is set to 5, 10, 15, and 20 N (Correspondingly 0.2, 0.4, 0.6, and 0.8 MPa) with a stroke length of 20 mm to imitate the actual working conditions of the guide rail. Test at each speed and load lasts for 30 min during which the friction force and coefficient of friction are recorded. Each of the tests is repeated three times for the eight samples.

2 Results

At the dead centers of a reciprocating contact or when a tribological system stops and starts again, true solid-solid contacts occur. A single reciprocating stroke of the friction test of S1 is shown in Fig.3 with the speed of 1 mm/s and load of 0.2 MPa(The negative friction coefficient represents the return of the stroke). At the beginning of the stroke, a sudden rise of friction coefficient indicates that the driving force of the system is fighting against the static friction force. Then a peak reached indicates that the driving force is equal to the static friction force and the peak of friction coefficient curve is the coefficient of static friction. Subsequently, the friction coefficient curve decreases and becomes stable, and at that time the coefficient of dynamic friction is obtained. It can be clearly observed that there is a difference between the dynamic and static friction coefficients which is the core factor that causes the stick-slip phenomenon.

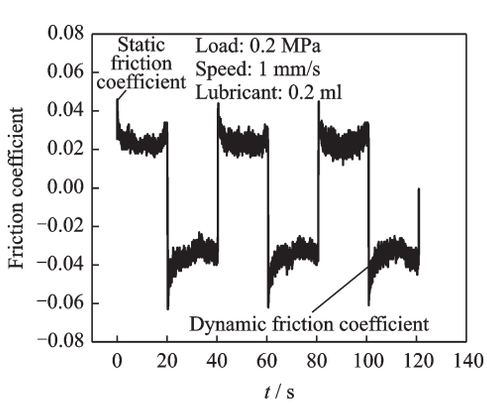

Fig.3 Friction coefficient curve of reciprocating strokes

2.1 Friction behaviors of eight samples under different speeds

The combination of static friction coefficient curves under different sliding speeds (0.1, 0.5, 1.0, 5.0, and 10.0 mm/s) are shown in Fig. 4. With the increase of the sliding speed, the static friction coefficient curves of S1, S5, S6, S7, and S8 show a trend of falling slightly first from 0.1 mm/s to 0.5 mm/s, then rising from 0.5 mm/s to 5 mm/s where obtain the highest static friction coefficient and then falling sharply. And the static friction coefficient curves of S2 and S3 show a continuous dropping process. Under low speed conditions, large area ratio textured samples such as S5 (area ratio of 19.6%) and S6 (area ratio of 28.26%) perform better and obtain a smaller static friction coefficient, while under high speed conditions, small area ratio textured samples such as S2 (area ratio of 3.14%) perform better and obtain a lower static friction coefficient.

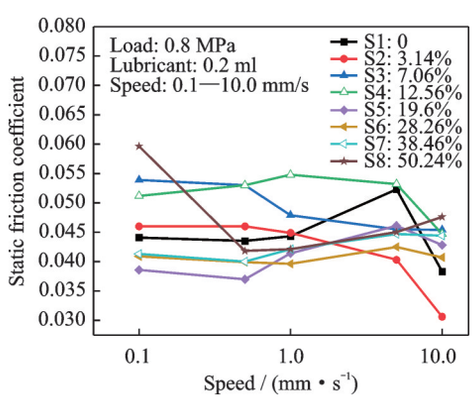

Fig.4 Coefficient of static friction under different speeds

The combination of dynamic friction coefficient curves under different sliding speeds (0.1, 0.5, 1.0, 5.0, and 10.0 mm/s) are shown in Fig.5. With the increase of the sliding speed, the curves of S1, S5, and S6 show a trend of rising first from 0.1 mm/s to 5 mm/s where the samples obtain the highest dynamic friction coefficient and falling from 5 mm/s to 10 mm/s. The curves of S2, S3, and S4 show a trend of rising first from 0.1 mm/s to 1 mm/s where the samples obtain the highest dynamic friction coefficient and falling from 1 mm/s to 10 mm/s under which the dynamic friction coefficients of the

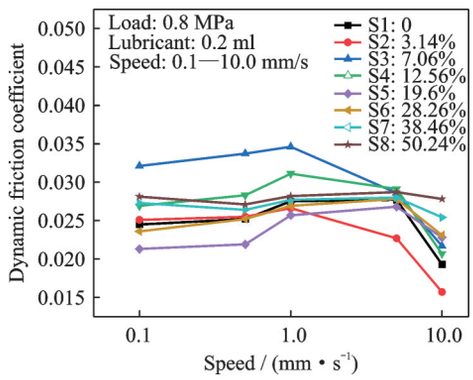

Fig.5 Coefficient of dynamic friction under different speeds

samples are the lowest compared with other conditions of sliding speed. The curves of S7 and S8 show a trend of falling first from 0.1 mm/s to 0.5 mm/s and rising from 0.5 mm/s to 5 mm/s where the samples obtain the highest dynamic friction coefficient and falling slightly from 5 mm/s to 10 mm/s. Under low speed conditions, large area ratio textured samples such as S5(area ratio of 19.6%) and S6(area ratio of 28.26%) perform better and obtain a smaller dynamic friction coefficient, while under high speed conditions, small area ratio textured samples such as S2(area ratio of 3.14%) perform better and obtain a lower dynamic friction coefficient.

Fig.6 shows the difference between the static and dynamic friction coefficients under different sliding speeds (0.1, 0.5, 1.0, 5.0, and 10.0 mm/s). With the increase of sliding speed, the difference of S2 keeps falling and obtains the difference of 0.017 6 and 0.014 9 decreasing by 28.46% and 21.58%, compared with S1 of 0.024 6 and 0.019 under the sliding speeds of 5 mm/s and 10 mm/s where the difference of S2 is lower than that of S1, respectively. The change trends of S5, S6, S7, and S8 are falling from 0.1 mm/s to 1 mm/s and then rising from 1 mm/s to 10 mm/s. During all the sliding speed conditions, S7 has the lowest difference under 0.1 mm/s and 0.5 mm/s of 0.014 and 0.013 7 decreasing by 28.57% and 25.14% compared with S1 of 0.019 6 and 0.018 3, respectively. S6 has the lowest difference under 1 mm/s and 5 mm/s of 0.012 7 and 0.014 7 decreasing by 24.4% and 40.24% compared with S1 of 0.016 8 and 0.024 6, respectively. The difference of S4 is always higher than that of S1 under all sliding speed conditions shown in Fig.6.

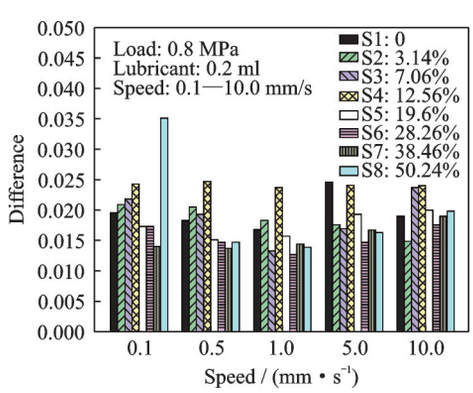

Fig.6 Difference between static and dynamic friction coefficients under different speeds

2.2 Friction behaviors of eight samples under typical conditions

Fig.7 shows the dynamic friction coefficients, static friction coefficients, and difference between static and dynamic friction coefficients of eight samples under different speeds and loads. The value corresponding to the upper end of the line segment represents the static friction coefficient, the lower end represents the dynamic friction coefficient, and the length of the line segment represents the difference between the dynamic and static friction coefficients. Under low-speed and light-load conditions (Fig.7

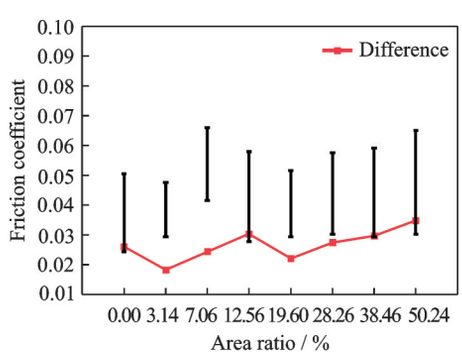

(a) 0.1 mm/s and 0.2 MPa

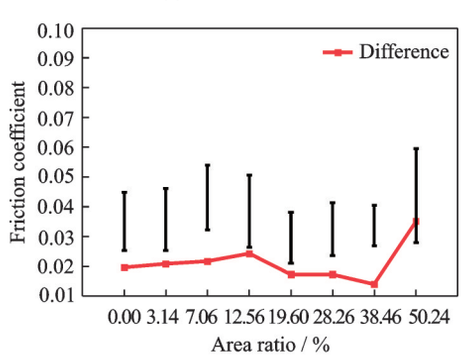

(b) 0.1 mm/s and 0.8 MPa

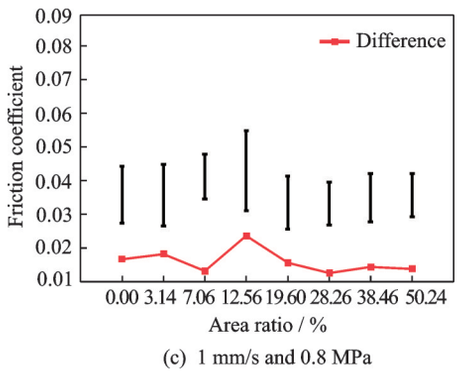

(c) 1 mm/s and 0.8 MPa

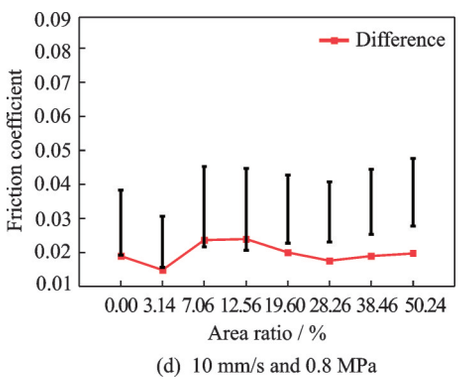

(d) 10 mm/s and 0.8 MPa

Fig.7 Dynamic friction coefficient, static friction coefficient and difference between them of eight samples under four typical conditions

(a)), S2(area ratio of 3.14%) reaches the lowest difference between static and dynamic friction coefficients and the other samples reach a higher difference compared with S1. Under low-speed and heavy-load conditions(Fig.7(b)), S7(area ratio of 38.46%) reaches the lowest difference between static and dynamic friction coefficient and S5(area ratio of 19.6%) and S6(area ratio of 28.26%) reduce the difference between the dynamic and static friction coefficients while reducing the dynamic and static friction coefficients. Under middle-speed and heavy-load conditions (Fig.7(c)), S6 (area ratio of 28.26%) reduces the lowest difference between the dynamic and static friction coefficients while reducing the dynamic and static friction coefficients and S6—S8 reach a lower difference compared with S1. Under high-speed and heavy-load conditions(Fig.7(d)), S2(area ratio of 3.14%) reduces the lowest difference between the dynamic and static friction coefficients while reducing the dynamic and static friction coefficients.

3 Discussion

The first is the mechanism of the effect of surface texture on the coefficient of dynamic friction. For a smooth surface(S1), as the upper sample slides on the lower guide rail, high pressure and low speed will squeeze out the lubricating oil from the contact surface, which causes the thickness of oil film to become thin or even destroyed, resulting in an increase in the coefficient of dynamic friction. For surface textured samples, the micro-dimples on the surface of the samples play the role of storing lubricants. During the sliding process, the micro-dimples constantly provide lubricants to the contact surface. As a result, the thickness of oil film becomes thick and rebuilt, resulting in a decrease in the coefficient of dynamic friction. Also, it is assumed that dimpled surfaces extend the range of hydrodynamic lubrication. However, the micro-dimples on the surface of the samples can also introduce concentrated stress at the edge of the dimples, resulting in an increase in the coefficient of dynamic friction. These mechanisms compete with each other, resulting in some area ratios of textured samples to lower the coefficient of dynamic friction, while other area ratios of textured samples increase the coefficient of dynamic friction.

Mechanism of surface texture affecting static friction coefficient are shown as follows. During the reciprocating tests, at the dead centers of reciprocating motion or when the stop and start states of the machine tool slide are switched, the hydrodynamic lubrication does not exist and solid-solid contact occurs between the two friction pairs. Based on the interface between the HT250 guide rail(lower sample) and PTFE belt(upper sample), we consider a mode Ⅱ crack (slip fracture) movement as a transition process from static friction to dynamic friction. Compared with a smooth surface, processing a micro-dimples texture on the surface of PTFE by LST, when mode Ⅱ crack occurs, due to the concentrated stress generated at the edge of the dimples, each dimple helps to initiate shear cracks; in addition, each dimple will increase the length of the crack, thereby increasing the driving force for crack extension, causing the reduction of the static friction

coefficient. However, when the crack is leaving the dimple, the dimples on the surface of the sample will pin the crack at the position of the dimple, which prevents the crack from continuing to extend. At the rear edge of the dimple, in addition to the stress concentration in the shear direction (type Ⅱ direction), the normal load of contact and the geometry of the dimple will also cause the stress concentration in the negative direction of the mode Ⅰ crack. This stress can be calculated using the following formula, proposed by Inglis[22]

$$\sigma_{yy} = \sigma_1(1 + 2(c/b)) \quad (1)$$

where σ_1 is the applied tension; b and c are the semi-principal coordinates of the elliptical hole, here c is the diameter of the dimple and b the depth of dimple. This is the reason why the textured area ratio is large (S7 and S8) but the static friction coefficient is higher than that of a smooth surface. The front of longer crack in the interface will be associated with higher system energy, and the "line tension" can be attributed to cracks similar to Orowan's dislocation model 2, indicating that the increase in shear tension $\Delta\tau$ makes the dislocation move through the crystal and is proportional to $1/L$, where L is the distance between obstacles which will pin the dislocations[23]. Here, the distance between obstacles is the distance between the dimples. This can also explain why the static friction coefficient of the sample S2 with a textured area ratio of 3.14% is small. Ben-David and Fineberg proposed that there would be a great reduction of the threshold for fracture if the "seed" crack was increased[24]. Here, the dimples on the surface of the samples play the role of the "seeds", the more the dimples are and the longer the dimples are, the lower the static friction coefficient is.

Considering all the above mechanisms, there will be an optimal textured area ratio that minimizes the static friction coefficient which are S5 (area ratio of 19.6%).

4 Conclusions

Reciprocating friction tests are successfully carried out under boundary lubrication and different area ratio patterns are fabricated by LST on the surface of upper samples. The results indicated that surface textures can significantly reduce the difference between the static and the dynamic friction coefficients and inhibit the stick-slip phenomenon of the guide rail. Regarding the tribological performance, we obtain the following conclusions:

(1) Under different speeds and load conditions, surface textures with different area ratios improve the tribological properties differently. Under low-speed-light-load and high-speed-heavy-load conditions, low area ratio textured sample S2 (area ratio of 3.14%) can better improve the tribological properties. Under low speed and heavy load conditions, large area ratio textured samples S5 (area ratio of 19.6%) and S6 (area ratio of 28.26%) can better improve the tribological properties.

(2) Surface textures can significantly reduce the static fiction coefficient. Under 0.1 mm/s and 0.6 MPa, S5 and S6 show the static friction coefficients of 0.040 1 and 0.041 4, decreased by 20.74% and 18.22, respectively, compared with S1 of 0.050 6. Under 0.1 mm/s and 0.6 MPa, S2 has the lowest static friction coefficient of 0.040 3 decreased by 22.9% compared with S1 of 0.052 3.

(3) Surface textures can significantly inhibit the stick-slip phenomenon of the guide rail. Under 0.1 mm/s and 0.2 MPa, S2 obtains the minimum difference of 0.018 2 between the static and the dynamic friction coefficients, decreased by 30.27% compared with S1 of 0.026 1. Under 5 mm/s and 0.8 MPa, S6 has the minimum difference of 0.014 7 between the static and the dynamic friction coefficients, decreased by 40.24% compared with S1 of 0.024 6.

References

[1] YUE H, DENG J X, GE D, et al. Effect of surface texturing on tribological performance of sliding guideway under boundary lubrication[J]. Journal of Manufacturing Processes, 2019, 47(1): 172-182.

[2] ZENG S, LI J, ZHOU N, et al. Improving the wear resistance of PTFE-based friction material used in ultrasonic motors by laser surface texturing[J]. Tribology International, 2020, 141(1): 105910.

[3] ZHANG Liping, LI Yenong, ZHAO Jianjie. Grey prediction on straightness errors of the plastic coated

guide rail of a CNC lathe[J]. Manufacturing Technology & Machine Tool, 2016(4): 38-41. (in Chinese)

[4] ZULEEG J. How to measure, prevent, and eliminate stick-slip and noise generation with lubricants[C]// Proceedings of SAE 2015 Noise and Vibration Conference and Exhibition. [S.l.]: SAE, 2015.

[5] BOWDEN F P. The friction and lubrication of solids[J]. American Journal of Physics, 1951, 19(7): 428.

[6] BELL R, BURDEKIN M. An investigation into the steady: Tate characteristics of plain slideways[J]. ARCHIVE Proceedings of the Institution of Mechanical Engineers, 1969, 184: 1075-1087.

[7] BELL R, BURDEKIN M. A study of the stick-slip motion of machine tool feed drives[J]. ARCHIVE Proceedings of the Institution of Mechanical Engineers, 1969, 184: 543-560.

[8] PERSSON B. Adhesion between an elastic body and a randomly rough hard surface[J]. The European Physical Journal E, 2002, 8(4): 385-401.

[9] IBRAHIM R A. Friction-induced vibration, chatter, squeal, and chaos—Part I: Mechanics of contact and friction[J]. Applied Mechanics Reviews, 1994, 47(7): 227.

[10] OKAN B, OMER A. Computer simulation of stick-slip motion in machine tool slideways[J]. Tribology International, 2004, 37(4): 347-351.

[11] HAMILTON D B, WALOWIT J A, ALLEN C M. A theory of lubrication by microirregularities[J]. Trans Asme Journal of Basic Eng, 1966, 88(1): 177-185.

[12] ANNO J N, WALOWIT J, ALLEN C M. Microasperity lubrication[J]. Lubrication Technol, 1968, 4(2): 351-355.

[13] FOWELL M T, MEDINA S, OLVER A V, et al. Parametric study of texturing in convergent bearings—ScienceDirect[J]. Tribology International, 2012, 52(3): 7-16.

[14] KLIGERMAN Y, ETSION I, SHINKARENKO A. Improving tribological performance of piston rings by partial surface texturing[J]. Journal of Tribology, 2005, 127(3): 632-638.

[15] PETTERSSON U, JACOBSON S. Textured surfaces for improved lubrication at high pressure and low sliding speed of roller/piston in hydraulic motors[J]. Tribology International, 2007, 40(2): 355-359.

[16] MURTHY A N, ETSION I, TALKE F E. Analysis of surface textured air bearing sliders with rarefaction effects[J]. Tribology Letters, 2007, 28(3): 251-261.

[17] ETSION I. Modeling of surface texturing in hydrodynamic lubrication[J]. Friction, 2013, 1(3): 195-209.

[18] ZHANG H, HUA M, DONG G W, et al. Boundary slip surface design for high speed water lubricated journal bearings[J]. Tribology International, 2014, 79(1): 32-41.

[19] CHENG H, GUO C X. Bionic design inspired by surface texture of Cybister's elytra[J]. Transactions of Nanjing University of Aeronautics and Astronautics, 2018, 35(S1): 55-62.

[20] GACHOT C, ROSENKRANZ A, HSU S M, et al. A critical assessment of surface texturing for friction and wear improvement[J]. Wear, 2017, 372(1): 21-41.

[21] WANG H, XIE X, HUA X, et al. The effect of laser surface texturing to inhibit stick-slip phenomenon in sliding contact[J]. Advances in Mechanical Engineering, 2019. DOI: 10.1177/1687814019874635.

[22] INGLIS C E. Stresses in a plate due to the pressence of cracks and sharp corners[C]//Proceedings of Spring Meetings of the 54th Session of the Institution of Naval Architects. [S.l.]: [s.n.], 1913.

[23] HULL D, BACON D J. Introduction to dislocations [M]. 5th ed. Amsterdam: Elsevier, 2011.

[24] BEN-DAVID O, FINEBERG J. Static friction coefficient is not a material constant[J]. Phys Rev Lett, 2011, 106(25): 254301.

Acknowledgement This work was financially supported by the National Natural Science Foundation of China (No. 51675268).

Author Mr. **LEI Ming** received the B.E. and M.E. degrees in mechanical engineering from Nanjing University of Aeronautics and Astronautics in 2017 and 2021, respectively. His interest focuses on the surface technology.

Author contributions Mr. **LEI Ming** designed the study, conducted the analysis and wrote the manuscript. Profs. **WANG Xiaolei** and **HUANG Wei** revised and modified the manuscript. All authors commented on the manuscript draft and approved the submission.

Competing interests The authors declare no competing interests.

(Production Editor: XU Chengting)

激光表面织构化PTFE在边界润滑条件下防爬行现象作用研究

雷 鸣，王晓雷，黄 巍
（南京航空航天大学机电学院，南京 210016，中国）

摘要：机床处于刚启动或者将要停止阶段会出现爬行现象，此时无法保证机床的高精度定位、加工精度和微动进给，其最关键的原因是动摩擦系数和静摩擦系数之间存在差值。本文利用激光表面织构技术在PTFE基复合材料表面加工不同面积率的圆坑织构，并且在边界润滑条件和面对面接触摩擦形式下，使用往复式摩擦试验机进行摩擦试验。结果表明，织构面积率为19.6%时可以最大限度地减小动摩擦系数和静摩擦系数之间的差值。

关键词：机床导轨；激光表面织构技术；爬行现象；动静摩擦系数之差